Springer Proceedings in Advanced Robotics 4
Series Editors: Bruno Siciliano · Oussama Khatib

Jadran Lenarčič
Jean-Pierre Merlet *Editors*

Advances in Robot Kinematics 2016

spar

Springer

Springer Proceedings in Advanced Robotics 4

More information about this series at http://www.springer.com/series/15556

Jadran Lenarčič · Jean-Pierre Merlet
Editors

Advances in Robot Kinematics 2016

Springer

Editors
Jadran Lenarčič
Jožef Stefan Institute
Ljubljana
Slovenia

Jean-Pierre Merlet
INRIA Sophia Antipolis
Sophia Antipolis Cedex
France

ISSN 2511-1256 ISSN 2511-1264 (electronic)
Springer Proceedings in Advanced Robotics
ISBN 978-3-319-56801-0 ISBN 978-3-319-56802-7 (eBook)
DOI 10.1007/978-3-319-56802-7

Library of Congress Control Number: 2017940802

Printed on acid-free paper

This Springer imprint is published by Springer Nature
The registered company is Springer International Publishing AG
The registered company address is: Gewerbestrasse 11, 6330 Cham, Switzerland

Foreword

Robots! Robots on Mars and in oceans, in hospitals and homes, in factories and schools; robots fighting fires, making goods and products, saving time and lives. Robots today are making a considerable impact from industrial manufacturing to health care, transportation, and exploration of the deep space and sea. Tomorrow, robots will become pervasive and touch upon many aspects of modern life.

The *Springer Tracts in Advanced Robotics (STAR)* was launched in 2002 with the goal of bringing to the research community the latest advances in the robotics field based on their significance and quality. During the latest fifteen years, the STAR series has featured publication of both monographs and edited collections. Among the latter, the proceedings of thematic symposia devoted to excellence in robotics research, such as ISRR, ISER, FSR, and WAFR, have been regularly included in STAR.

The expansion of our field as well as the emergence of new research areas has motivated us to enlarge the pool of proceedings in the STAR series in the past few years. This has ultimately led to launching a sister series in parallel with STAR. The *Springer Proceedings in Advanced Robotics (SPAR)* is dedicated to the timely dissemination of the latest research results presented in selected symposia and workshops.

This volume of the SPAR series brings the proceedings of the fifteenth edition of ARK on Advances in Robot Kinematics, whose proceedings have been previously published by Kluwer and Springer since 1991. This edition took place in Grasse, France, from June 27 to June 30, 2016. The volume edited by Jadran Lenarčič and Jean-Pierre Merlet contains 46 scientific contributions, revised and extended after the meeting. This collection focuses on mechanism and kinematics with special emphasis on parallel robots, control, and singularities.

From its excellent technical program to its warm social interaction, ARK culminates with this unique reference on the current developments and new advances in robot kinematics—a genuine tribute to its contributors and organizers!

Naples, Italy — Bruno Siciliano
Stanford, CA, USA — Oussama Khatib
March 2017 — SPAR Editor

Preface

Kinematics, the motion of mechanisms, is one of the most fundamental aspects of robot design, analysis, and control, but it is also relevant to other scientific domains, such as biomechanics, molecular biology, and others. This series of books on Advances in Robot Kinematics, which reports the latest achievements in the field, has a long history, as the first symposium was organized in 1988, and the first book was published by Springer in 1991. Since then, a new issue has been published every two years. Each book is linked to a single-track symposium in which the participants exchange their results and opinions in a meeting that brings together the world's best researchers and scientists as well as young students. Since 1992, these symposia have come under the patronage of the International Federation for the Promotion of Machine Science (IFToMM).

In 2016, the symposium related to this book was organized by the French National Research Institute in Computer Science and Control Theory (INRIA) in Grasse, France. We are grateful to the authors for their contributions and to the large team of reviewers for their critical and insightful recommendations. The papers in this book show that robot kinematics is an exciting domain with an enormous number of research challenges that go well beyond the field of robotics. We are also indebted to the members of the HEP-HAISTOS team of INRIA for their help in organizing the symposium. The articles from this symposium were first published in a green open-access archive to favor the free dissemination of the results. We are grateful to Y. Papegay for putting the edition together.

The current book is the 13th in the series of Springer (and Kluwer) and is the result of a peer-review process intended to select the newest and most original achievements in this field. The book was published after the conference. This was unusual for the series from the symposia Advances in Robot Kinematics, because the books are typically released before the conference. However, this circumstance allowed the authors to have their manuscripts further improved and to take into account the opinions and constructive criticisms of the conference participants. Some authors even made re-calculations and produced new and more valuable results.

First and foremost, we are grateful to the authors who participated in this project with all their enthusiasm and commitment. We are grateful to Springer, to the whole team, but especially to Nathalie Jacobs and Cynthia Feenestra, who have made this publication possible. Above all, we are grateful to our younger colleague Tadej Petrič, Ph.D., whose assistance was crucial in the technical production of the book. Without him, things would not have taken place as efficiently and rapidly.

We hope that our book will again reach the shelves of scholars, researchers, and students around the world who are attracted to the unique field of robot kinematics.

Ljubljana, Slovenia
September 2016

Jadran Lenarčič
Jean-Pierre Merlet

Contents

Mass Equivalent Pantographs for Synthesis of Balanced Focal Mechanisms

Volkert van der Wijk

Abstract Force balance is an important property in the design of high-speed high precision machinery to reduce base vibrations and also for the design of inherently safe large movable structures. This paper presents the synthesis of inherently balanced overconstrained focal mechanisms with mass equivalent pantographs. It is shown how pantograph linkages can be combined into an overconstrained but movable linkage by connecting them in their similarity points. With mass equivalent modeling the force balance conditions are derived for which the common center of mass is in the focal point for any motion. As examples, Burmester's focal mechanism is investigated for balance and a new balanced focal mechanism of three mass equivalent pantographs is presented.

1 Introduction

In robotics, dynamic (shaking) force balance is an important property for high-speed motion with minimal base vibrations [4]. Since force balanced mechanisms are statically balanced too, it is also a useful property for large moving structures for save motion with minimal effort.

A problem of common approaches to balance pre-existing mechanisms is that generally a multitude of counter-masses is required [1, 9], leading to unpractical designs with a significant increase of mass and inertia [6]. Instead, a reversed approach was presented where balanced mechanisms are synthesized from inherently balanced linkage architectures [4]. These linkage architectures consist solely of the essential

V. van der Wijk (✉)
Mechatronic System Design, Department of Precision and Microsystems Engineering,
Faculty of Mechanical, Maritime, and Materials Engineering, Delft University of Technology,
Mekelweg 2, Delft, The Netherlands
e-mail: V.vanderWijk@tudelft.nl; Volkert.vanderWijk@kcl.ac.uk

V. van der Wijk
Centre for Robotics Research, Department of Informatics,
Faculty of Natural and Mathematical Sciences, King's College London,
Strand, London, UK

J. Lenarčič and J.-P. Merlet (eds.), *Advances in Robot Kinematics 2016*,
Springer Proceedings in Advanced Robotics 4, DOI 10.1007/978-3-319-56802-7_1

kinematic relations for balance. With this method a variety of new advantageous inherently balanced mechanism solutions were found among which the first high-speed dynamically balanced parallel manipulator that was successfully built and tested [8].

With inherent balancing it is also possible to synthesize balanced mechanism solutions from *overconstrained* inherently balanced linkage architectures [7]. These architectures have more links than kinematically needed. This gives the designer the freedom to select links to keep or eliminate to obtain a normally constrained balanced mechanism solution. Also more solutions can potentially be found.

The goal of this paper is to investigate focal mechanisms, which are overconstrained and movable, for inherent balance. The focal mechanism of Burmester [2] - the cognate of Kempe's focal mechanism - can be regarded a combination of two pantographs [3]. It is shown how these two pantograph linkages can be combined by connecting them in their similarity points. For force balance the two pantographs need to be mass equivalent with a model of which the common center of mass (CoM) is in the focal point. The conditions for this are derived. In addition also a new inherently balanced focal mechanism of three combined pantographs is presented at the end.

2 CoM in Focal Point of Burmester's Focal Mechanism

Figure 1 shows Burmester's focal mechanism which consists of the two pantograph linkages $P_1A_1P_2S$ - with link lengths l_1, l_2, a_1, and a_2 - and $P_3A_3P_4S$ - with link lengths l_3, l_4, a_3, and a_4 - that are connected with revolute pairs in the similarity points A_0, A_2, and S. This linkage is two times overconstrained yet movable since both pantographs are similar, i.e. elements $A_0A_1P_1 \sim A_1A_2P_2 \sim A_0A_3P_3 \sim A_3A_2P_4$ with angles β_1 and β_2. These four triangular elements are also similar to triangle A_0A_2S for

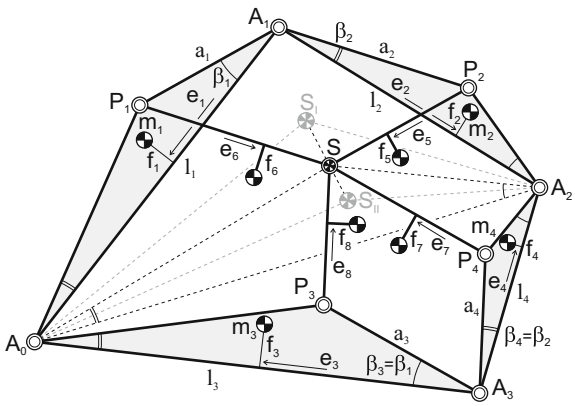

Fig. 1 Burmester's focal mechanism of two pantograph linkages connected in their similarity points A_0, A_2, and S. S is the focal point and is the common CoM of all elements for force balance

any motion of the mechanism. Both pairs of opposite internal four-bars are reflected similar to one another, with one pair being parallelograms.

When, for example, for the upper pantograph a_1, a_2, l_1, and β_1 are given, l_2 and β_2 can be calculated as

$$\lambda_1^S = 1 - \frac{a_1}{l_1}\cos\beta_1, \quad \lambda_2^S = \frac{a_1}{l_1}\sin\beta_1 \tag{1}$$
$$\beta_2 = \tan^{-1}\frac{\lambda_2^S}{\lambda_1^S}, \quad l_2 = \frac{a_2}{\lambda_1^S}\cos\beta_2 = \frac{a_2}{\lambda_2^S}\sin\beta_2$$

with λ_1^S and λ_2^S the constant similarity parameters of the four triangular elements and triangle A_0A_2S. When, subsequently, for the lower pantograph l_3 and l_4 are given, a_3 and a_4 can be calculated as

$$a_3 = (1-\lambda_1^S)\frac{l_3}{\cos\beta_1} = \lambda_2^S\frac{l_3}{\sin\beta_1}, \quad a_4 = l_4\frac{\lambda_1^S}{\cos\beta_2} = l_4\frac{\lambda_2^S}{\sin\beta_2} \tag{2}$$

These parameters can also be obtained from the similarity conditions of the four triangular elements which write

$$\frac{a_1}{l_1} = \frac{a_3}{l_3}, \quad \frac{a_2}{l_2} = \frac{a_4}{l_4} \tag{3}$$

In Fig. 1 each of the eight links i has a mass m_i of which the CoM is defined with parameters e_i and f_i as illustrated. The aim is to design the mechanism such that the common CoM of all elements is in focal point S for any motion. Then the mechanism is inherently force balanced with respect to the focal point.

The force balance conditions describe how the CoM parameters of each element are related for balance. These conditions can be found by mass equivalent modeling with real and virtual equivalent masses [4, 5]. With mass $m_I = m_1 + m_2 + m_5 + m_6$ of upper pantograph $P_1A_1P_2S$ and mass $m_{II} = m_3 + m_4 + m_7 + m_8$ of lower pantograph $P_3A_3P_4S$ the total mass of the focal mechanism can be written as $m_{tot} = m_I + m_{II}$. The common CoM of the upper pantograph is denoted S_I and the common CoM of the lower pantograph is denoted S_{II}. With similarity points A_0 and A_2 these two points form two triangles as well which also have to remain similar for any motion. For force balance then each pantograph is mass equivalent to a 2-DoF mass equivalent model with the conditions [5]

$$m_I^a = m_I(1-\lambda_1^I), \quad m_I^b = m_I\lambda_1^I, \quad m_I^c = m_I\lambda_2^I \tag{4}$$
$$m_{II}^a = m_{II}(1-\lambda_1^{II}), \quad m_{II}^b = m_{II}\lambda_1^{II}, \quad m_{II}^c = m_{II}\lambda_2^{II}$$

with λ_1^I and λ_2^I the similarity parameters of triangle $A_0A_2S_I$, λ_1^{II} and λ_2^{II} the similarity parameters of triangle $A_0A_2S_{II}$, and real equivalent masses m_j^a and m_j^b and virtual equivalent mass m_j^c of each pantograph j. For the upper pantograph in Fig. 2a, b shows the 2-DoF mass equivalent model adapted from [5]. Essentially the virtual

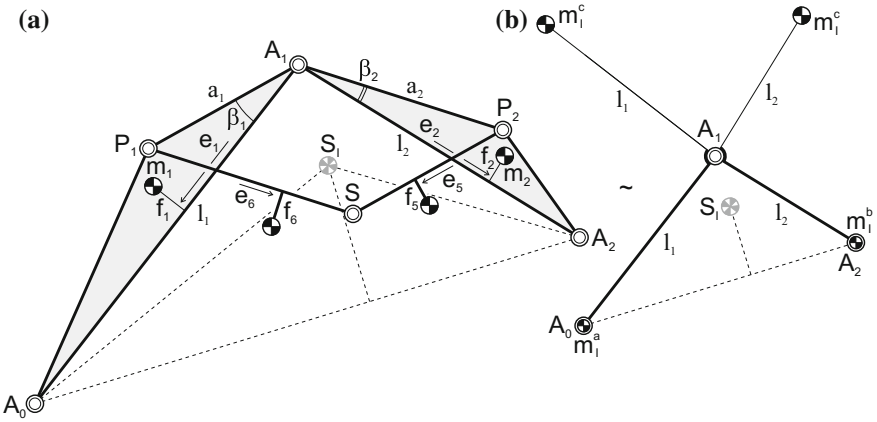

Fig. 2 For force balance (**a**) each pantograph must be mass equivalent to the (**b**) 2-DoF mass equivalent model, here shown for the upper pantograph with CoM in S_I

equivalent mass determines the link CoMs relative to the lines connecting the joints, i.e. the values of parameters f_i, whereas the real equivalent masses determine the link CoMs along the lines connecting the joints, i.e. the values of parameters e_i.

To have the common CoM in the focal point, the sum of the mass equivalent models of the two pantographs should equal the mass equivalent model of the complete mechanism. This can be written as $m_I\lambda_1^I + m_{II}\lambda_1^{II} = m_{tot}\lambda_1^S$ and $m_I\lambda_2^I + m_{II}\lambda_2^{II} = m_{tot}\lambda_2^S$. The resulting model is similar to Fig. 2b but with each equivalent mass replaced with the sum of the equivalent masses of the two pantograph models as $m^a = m_I^a + m_{II}^a, m^b = m_I^b + m_{II}^b$, and $m^c = m_I^c + m_{II}^c$. The conditions for the mass equivalent model of the complete mechanism then are written as

$$m^a = m_{tot}(1 - \lambda_1^S), \quad m^b = m_{tot}\lambda_1^S, \quad m^c = m_{tot}\lambda_2^S \tag{5}$$

The force balance conditions for each pantograph can be derived from the linear momentum equations of each DoF individually where the linear momentum of the mass equivalent model must equal the linear momentum of the real pantograph, similar as for the dyads in [5]. Figure 3a shows the mass motions of DoF 1 of the upper pantograph where link A_1A_2 is fixed and link A_0A_1 rotates about A_1 with angle θ_{I1}. The mass motion of the pantograph for this DoF is shown on the right with a compact Equivalent Linear Momentum System (ELMS) where all masses are projected on element A_0A_1. Figure 3b shows the mass motions of DoF 2 where link A_1A_0 is fixed and link A_1A_2 rotates about A_1 with angle θ_{I2}. Also here the mass motion of the pantograph for this DoF is shown on the right with a compact ELMS where all masses are projected on element A_1A_2. The linear momentum L_1 and L_2 of these individual motions can be written with respect to their relative reference frames $x_{I1}y_{I1}$ and $x_{I2}y_{I2}$, which are aligned with lines A_0A_1 and A_2A_1, respectively, as

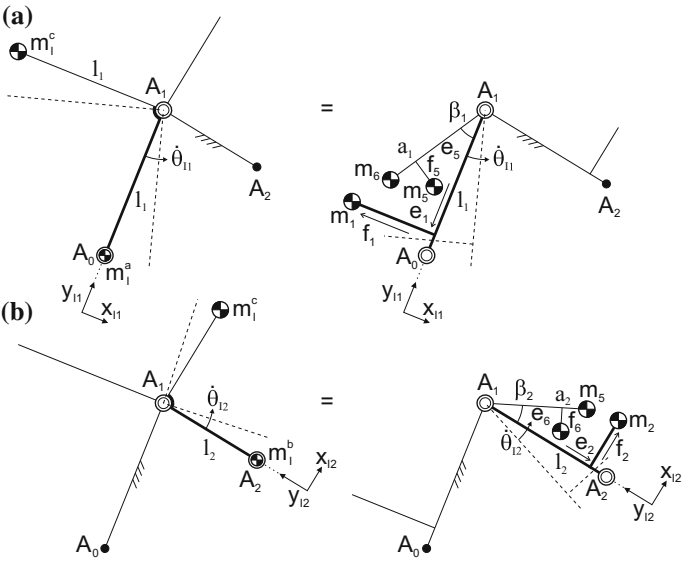

Fig. 3 The force balance conditions are derived from the linear momentum equations of each DoF individually which are equal for the mass equivalent model (*left*) and the real pantograph (*right*, here shown as compact Equivalent Linear Momentum Systems)

$$\frac{\overline{L}_1}{\dot{\theta}_{I1}} = \begin{bmatrix} m_I^a l_1 \\ -m_I^c l_1 \end{bmatrix} = \begin{bmatrix} m_1 e_1 + m_5(e_5 \cos\beta_1 + f_5 \sin\beta_1) + m_6 a_1 \cos\beta_1 \\ -m_1 f_1 - m_5(e_5 \sin\beta_1 - f_5 \cos\beta_1) - m_6 a_1 \sin\beta_1 \end{bmatrix} \quad (6)$$
$$\frac{\overline{L}_2}{\dot{\theta}_{I2}} = \begin{bmatrix} m_I^b l_2 \\ m_I^c l_2 \end{bmatrix} = \begin{bmatrix} m_2 e_2 + m_5 a_2 \cos\beta_2 + m_6(e_6 \cos\beta_2 + f_6 \sin\beta_2) \\ m_2 f_2 + m_5 a_2 \sin\beta_2 + m_6(e_6 \sin\beta_2 - f_6 \cos\beta_2) \end{bmatrix}$$

These equations result in the four force balance conditions

$$m_I^a l_1 = m_1 e_1 + m_5(e_5 \cos\beta_1 + f_5 \sin\beta_1) + m_6 a_1 \cos\beta_1 \quad (7)$$
$$m_I^c l_1 = m_1 f_1 + m_5(e_5 \sin\beta_1 - f_5 \cos\beta_1) + m_6 a_1 \sin\beta_1 \quad (8)$$
$$m_I^b l_2 = m_2 e_2 + m_5 a_2 \cos\beta_2 + m_6(e_6 \cos\beta_2 + f_6 \sin\beta_2) \quad (9)$$
$$m_I^c l_2 = m_2 f_2 + m_5 a_2 \sin\beta_2 + m_6(e_6 \sin\beta_2 - f_6 \cos\beta_2) \quad (10)$$

For the other pantograph the force balance conditions can be derived similarly as

$$m_{II}^a l_3 = m_3 e_3 + m_7(e_7 \cos\beta_1 + f_7 \sin\beta_1) + m_8 a_3 \cos\beta_1 \quad (11)$$
$$m_{II}^c l_3 = m_3 f_3 + m_7(e_7 \sin\beta_1 - f_7 \cos\beta_1) + m_8 a_3 \sin\beta_1 \quad (12)$$
$$m_{II}^b l_4 = m_4 e_4 + m_7 a_4 \cos\beta_2 + m_8(e_8 \cos\beta_2 + f_8 \sin\beta_2) \quad (13)$$
$$m_{II}^c l_4 = m_4 f_4 + m_7 a_4 \sin\beta_2 + m_8(e_8 \sin\beta_2 - f_8 \cos\beta_2) \quad (14)$$

These are the 8 general force balance conditions of the focal mechanism in Fig. 1 for which the common CoM is in the focal point S. For example, from the first four equations the equivalent masses m_I^a, m_I^b, and m_I^c may be found to subsequently calculate with Eq. (5) the equivalent masses m_{II}^a m_{II}^b, and m_{II}^c to be used in the latter four balance conditions. It is also possible to initially choose values for m_I^a m_I^b, and m_I^c. Then for instance from the first four equations e_5, f_5, e_6, and f_6 can be derived as

$$e_5 = \frac{\sin\beta_1(m_I^c l_1 - m_1 f_1 - m_6 a_1 \sin\beta_1) + \cos\beta_1(m_I^a l_1 - m_1 e_1 - m_6 a_1 \cos\beta_1)}{m_5}$$

$$f_5 = \frac{\sin\beta_1(m_I^a l_1 - m_1 e_1 - m_6 a_1 \cos\beta_1) - \cos\beta_1(m_I^c l_1 - m_1 f_1 - m_6 a_1 \sin\beta_1)}{m_5}$$

$$e_6 = \frac{\sin\beta_2(m_I^c l_2 - m_2 f_2 - m_5 a_2 \sin\beta_2) + \cos\beta_2(m_I^b l_2 - m_2 e_2 - m_5 a_2 \cos\beta_2)}{m_6}$$

$$f_6 = \frac{\sin\beta_2(m_I^b l_2 - m_2 e_2 - m_5 a_2 \cos\beta_2) - \cos\beta_2(m_I^c l_2 - m_2 f_2 - m_5 a_2 \sin\beta_2)}{m_6}$$

3 Focal Mechanism of Three Pantographs

In general it is possible to synthesize a variety of inherently force balanced focal linkages by combining multiple mass equivalent pantographs in the same way as in the previous section. Figure 4 shows a new focal mechanism that is composed of the three pantographs $P_1A_1P_2S$, $P_3A_3P_4S$, and $P_5A_5P_6S$ which are connected in similarity points A_0, A_2, A_4, and S where S is the focal point. The resulting linkage is four times overconstrained yet movable. Also here each pantograph has similar triangular elements and a similar triangle of the similarity points. However in this case

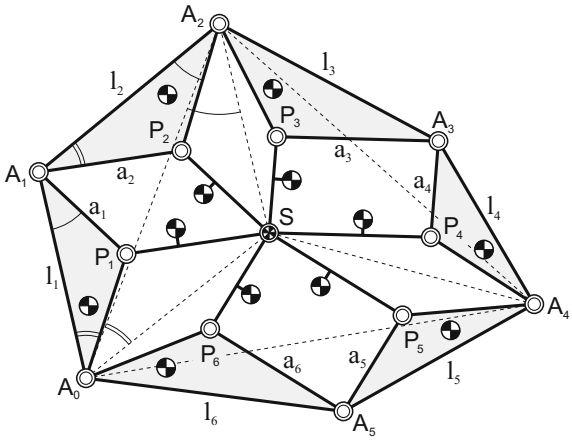

Fig. 4 Focal mechanism of three pantograph linkages connected in their similarity points A_0, A_2, A_4, and S. S is the focal point and is the common CoM of all elements for force balance

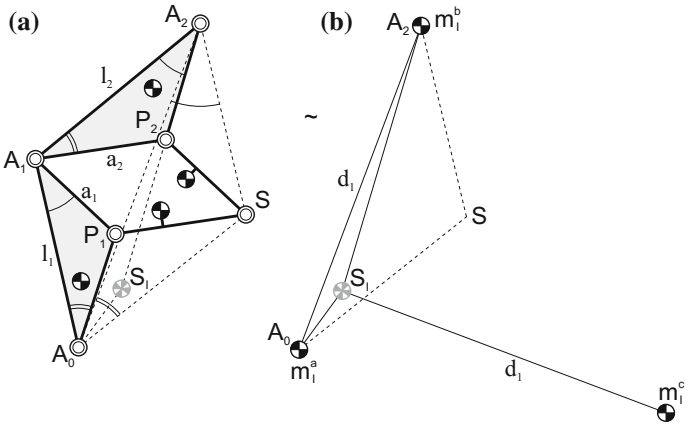

Fig. 5 (**a**) A pantograph with CoM in S_I can be modeled as a (**b**) mass equivalent single element with equivalent masses m_I^a, m_I^b, and m_I^c

the pantographs differ from one another, e.g. the triangular elements of pantograph $P_1A_1P_2S$ are not similar to the triangular elements of the other pantographs. In fact the focal mechanism is a combination of the three different triangles A_0A_2S, A_2A_4S, and A_0A_4S that together form the triangle $A_0A_2A_4$. For each pantograph the dimensions of the elements can be calculated with Eq. (1) with for each pantograph different λ^S parameters. For two pantographs the λ^S parameters can be chosen independently such that with the triangle $A_0A_2A_4$ the third is determined.

The approach to derive the force balance conditions for which the common CoM is in focal point S is similar to Burmester's focal mechanism. Here the mechanism can be considered a combination of three mass equivalent models with each a mass m_I, m_{II}, and m_{III} with CoMs in S_I, S_{II}, and S_{III}, respectively. For each pantograph the force balance conditions can be found with Eq. (6). The equivalent masses m_j^a, m_j^b, and m_j^c of each mass equivalent model are defined according to Eq. (4).

To find the mass equivalent model of the complete focal mechanism it is possible to model each pantograph as a mass equivalent single element as shown for pantograph $P_1A_1P_2S$ in Fig. 5. In Fig. 5b triangle $A_0A_2S_I$ can be regarded a rigid element with a real equivalent mass m_I^a in joint A_0, a real equivalent mass m_I^b in joint A_2, and a virtual equivalent mass m_I^c located at a distance d_1 from S_1, the CoM of the model, as illustrated. d_1 is equal to the distance between A_0 and A_2.

Combining the mass equivalent single elements of the three pantographs then results in the model in Fig. 6. This mass equivalent model of the complete focal mechanism has real equivalent masses $m_I^a + m_{III}^b$ in A_0, $m_I^b + m_{II}^a$ in A_2, and $m_{II}^b + m_{III}^a$ in A_4 and it has virtual equivalent masses m_I^c about S_I, m_{II}^c about S_{II}, and m_{III}^c about S_{III} as illustrated. Figure 7 shows the unified mass equivalent model of the complete focal mechanism. The difference with Fig. 6 is that here all the three virtual equivalent masses are located about S. From this model the conditions for which S is the CoM can be derived as

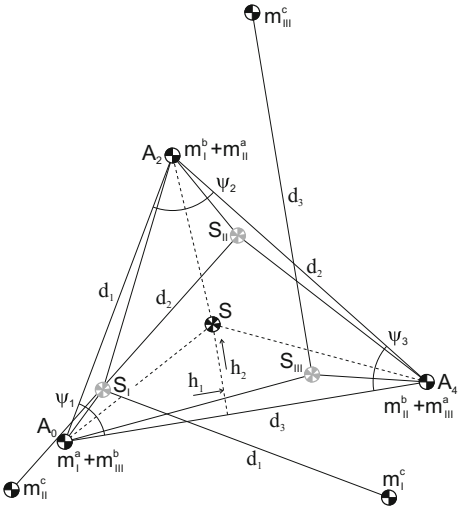

Fig. 6 Combination of the three mass equivalent single models with their equivalent masses. The common CoM of the focal mechanism is the CoM of this combined mass equivalent model

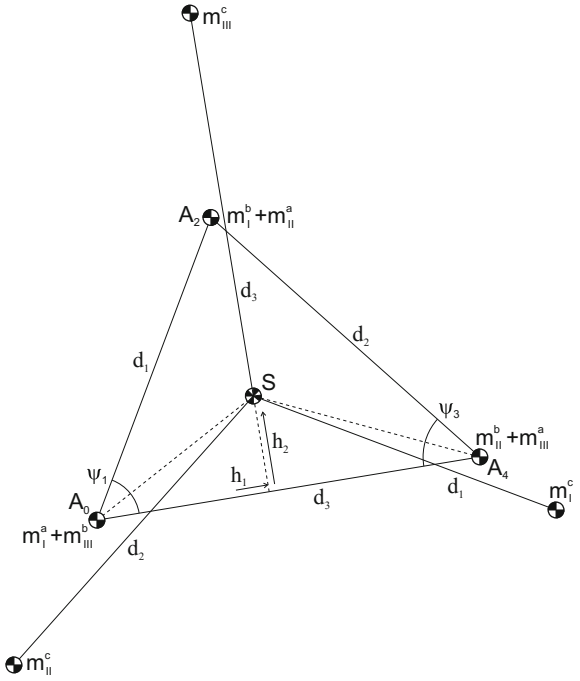

Fig. 7 The unified mass equivalent model of the focal mechanism in Fig. 4 with the CoM in *S* about which all three virtual equivalent masses are located

$$\begin{aligned}
&(m^b_{II} + m^a_{III})d_3 + (m^b_I + m^a_{II})d_1 \cos\psi_1 = m_{tot}h_1 \\
&(m^b_I + m^a_{II})d_1 \sin\psi_1 = m_{tot}h_2 \\
&m^c_{III}d_3 - m^c_{II}d_2 \cos\psi_3 - m^c_I d_1 \cos\psi_1 = 0 \\
&m^c_I d_1 \sin\psi_1 - m^c_{II}d_2 \sin\psi_3 = 0
\end{aligned} \tag{15}$$

with total mass $m_{tot} = m_I + m_{II} + m_{III}$ and with the CoM in S defined with respect to A_0A_4 by h_1 and h_2. The meaning of the first two conditions is that S is the CoM of the real equivalent masses, while the meaning of the last two conditions is that S is the CoM of the virtual equivalent masses.

4 Discussion and Conclusion

The inherent force balance of Burmester's focal mechanism was investigated and the force balance conditions were derived. It was shown that for balancing the focal mechanism can be considered composed of two mass equivalent pantographs. Combination of the mass equivalent models of the pantographs then results in one mass equivalent model of which the center of mass is in the focal point.

It was also shown how with three mass equivalent pantographs a new focal mechanism could be designed. In general, by combining multiple mass equivalent pantographs a variety of inherently balanced focal mechanisms can be synthesized. Unifying the mass equivalent models of all pantographs then results in a single mass equivalent model of which the center of mass is in the focal point.

Parameters a_i are the principal dimensions of the focal mechanism when its common center of mass is in the focal point. When the center of mass of an individual pantograph is in the focal point, then a_i are also the principal dimensions of this individual pantograph.

Although in Burmester's focal mechanism the two pantographs are in opposite branch, this is not required from the force balance conditions. This means that for force balance one of the pantographs or both of them may also be in the other branch, which means that they could also appear as being on top of one another.

Acknowledgements This publication was financially supported by the Niels Stensen Fellowship.

References

1. Briot, S., Bonev, I.A., Gosselin, C.M., Arakelian, V.: Complete shaking force and shaking moment balancing of planar parallel manipulators with prismatic pairs. Multi-Body Dyn. **223**(K), 43–52 (2009)
2. Burmester, L.: Die brennpunktmechanismen. Zeitschrift für Mathematik und Physik **38**, 193–223 and 3 appendices (1893)
3. Dijksman, E.A.: Motion Geometry of Mechanisms. Cambridge University Press (1979)

4. Van der Wijk, V.: Methodology for analysis and synthesis of inherently force and moment-balanced mechanisms - theory and applications (dissertation). University of Twente (free download: http://dx.doi.org/10.3990/1.9789036536301) (2014)
5. Van der Wijk, V.: Mass equivalent dyads. In: Bai, S., Ceccarrelli, M. (eds.) Recent Advances in Mechanism Design for Robotics. MMS 33, pp. 35–45. Springer, Berlin (2015)
6. Van der Wijk, V., Demeulenaere, B., Gosselin, C., Herder, J.L.: Comparative analysis for low-mass and low-inertia dynamic balancing of mechanisms. Mech. Robot. **4**(3), 031008 (2012)
7. Van der Wijk, V., Herder, J.L.: Inherently balanced 4R four-bar based linkages. In: Lenarčič, J., Husty, M. (eds.) Latest Advances in Robot Kinematics, Proceedings of the IFToMM 13th International Symposium on Advances in Robot Kinematics, pp. 309–316. Springer, Berlin (2012). ISBN 978-94-007-4619-0
8. Van der Wijk, V., Krut, S., Pierrot, F., Herder, J.L.: Design and experimental evaluation of a dynamically balanced redundant planar 4-RRR parallel manipulator. Int. J. Robot. Res. **32**(6), 744–759 (2013)
9. Wu, Y., Gosselin, C.M.: Design of reactionless 3-DOF and 6-DOF parallel manipulators using parallelepiped mechanisms. IEEE Trans. Robot. **21**(5), 821–833 (2005)

Compliant Serial 3R Chain with Spherical Flexures

Farid Parvari Rad, Rocco Vertechy, Giovanni Berselli and Vincenzo Parenti-Castelli

Abstract A spherical flexure is a special kind of compliant hinge specifically conceived for spherical motion. It features an arc of a circle as centroidal axis and an annulus sector as cross-section, circle and annulus having a common center coinciding to that of the desired spherical motion. This paper investigates a compliant spherical 3R open chain that is obtained by the in-series connection of three identical spherical flexures having coincident centers and mutually orthogonal axes of maximum rotational compliance. The considered spherical chain is intended to be used as a complex flexure for the development of spatial parallel manipulators. The compliance matrix of the proposed chain is first determined via an analytical procedure. Then, the obtained equations are used in a parametric study to assess the influence of spherical flexure geometry on the overall stiffness performances of the considered 3R open chain.

1 Introduction

Compliant mechanisms (CMs) are a special kind of articulated systems in which motion, force or energy are transferred or transformed through the deflection of flexible members (hereafter briefly referred to as "flexures" or "flexural hinges") [10]. Thanks to the absence (or reduced use) of traditional kinematic pairs, which are

F. Parvari Rad (✉) · R. Vertechy · V. Parenti-Castelli
Department of Industrial Engineering, University of Bologna, Bologna, Italy
e-mail: farid.parvarirad2@unibo.it

R. Vertechy
e-mail: rocco.vertechy@unibo.it

V. Parenti-Castelli
e-mail: vincenzo.parenti@unibo.it

G. Berselli
Department of Mechanical, Energy, Management and Transportation Engineering, University of Genova, Genova, Italy
e-mail: giovanni.berselli@unige.it

J. Lenarčič and J.-P. Merlet (eds.), *Advances in Robot Kinematics 2016*,
Springer Proceedings in Advanced Robotics 4, DOI 10.1007/978-3-319-56802-7_2

instead based on mating surfaces, CMs are almost not affected by wear, friction and backlash, and only require minimal maintenance with no need of lubrication. Due to their hinge-less nature, CMs can be manufactured in a single piece (for instance via laser or water jet cutting, electrical discharge machining or additive manufacturing), thereby reducing number of parts, assembly needs and, thus, manufacturing costs. With the above-mentioned features, CMs are ideal to work in vacuum, contamination-free, wet or dirty environments and in devices requiring resistance to shocks and silent operation. Common applications of CMs span high-precision manufacturing [27, 36], minimally invasive surgery [9, 18] and micro-electromechanical systems (MEMS) [1, 30].

As regards the existing literature, several studies have been devoted to the design, the characterization and the comparative evaluation of different flexure geometries and CMs formed therewith (see e.g. [14, 21, 31, 35]). In particular, most of these devices have been specifically conceived for the generation of planar motions only, out-of-plane displacements being regarded as *parasitic effects* to be minimized when possible [13]. On the other hand, despite the huge potentialities, exploitation and study of CMs specifically conceived for spatial motions have been much more rare (see e.g. [3–5, 20, 26, 28, 32, 34, 39]). Within this scenario, the development of Spherical CMs (SCMs) has recently attracted the attention of several researchers. SCMs are an important class of flexure-based spatial CMs in which all points of the end-link are ideally constrained to move on concentric spherical surfaces that are fixed with respect to the grounded link. In particular, the in-series ensemble of two or three compliant revolute (R) joints (of either planar notch, planar leaf spring or straight torsion beam type) with orthogonal and intersecting axes has been proposed in [8, 17, 19, 37] to conceive compliant spherical 2R or 3R serial chains to be used as compliant universal or spherical joints for the development of Cardan's [33] and Double-Hooke's couplings [17] and of spatial parallel manipulators [4, 5, 20, 26, 28, 32, 34, 39]. In these applications, the use of compliant spherical 2R or 3R serial chains in place of the axial-symmetric notch primitive flexure is usually preferred owing to the more limited ranges of motions and larger stress concentrations of this latter. The connection of four, five, six or eight bars with an equal number of compliant revolute joints (of either straight crease or lamina emergent torsional type) with intersecting axes has been considered in [6, 7, 38] for the development of 4R, 5R, 6R or 8R closed single-loop lamina-emergent SCMs, as well as arrays thereof (including the six bar Watt's and Stephenson's linkages), to be used in origami-inspired foldable systems such as pop-up books, industrial packaging and deployable devices. Planar notch and straight torsion beam flexures have been used in [19] to develop an actuated miniature 3-CRU (C and U denoting cylindrical and universal joints respectively) spherical parallel CM for the orientation of parts and tools in space. The in-parallel connection of three symmetrically placed spherical 3R serial chains employing either lamina emergent straight torsion beam or notch flexures has been proposed in [11, 29] for the development of 3-(3R) spherical parallel CMs with flat initial state to be used in compact pointing devices such as in MEMS beam-steering mirrors or medical instruments.

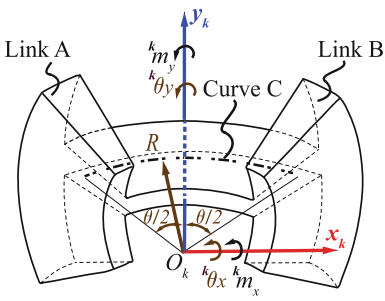

Fig. 1 Spherical flexures

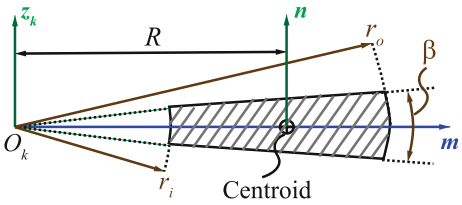

Fig. 2 Cross section properties of SFs

In all the above-mentioned studies, the considered SCMs have been obtained by employing compliant revolute flexures specifically conceived for planar motion applications. In contrast to this, Circularly-Curved Beam Flexures (CCBFs) with constant cross-section and featuring lower rotational rigidity along the radial direction have been proposed in [12, 22] for the development of SCMs with improved spherical motion capabilities. Among these CCBFs, those with annulus sector cross-section as depicted in Figs. 1 and 2, hereafter referred to as Spherical Flexures (SFs), have recently been demonstrated among the most effective ones in reducing the drift of the desired center of spherical motion under the combined action of torques and forces [25].

In this context, this paper investigates the use of SFs for the development of compliant spherical 3R serial chains to be used as SCMs or as spherical complex flexure components for spatial CMs with either serial or parallel architecture. As depicted in Fig. 3, the considered spherical chains are obtained by the in-series connection of three identical SFs that are arranged in space so as to share the same center of curvature and have mutually orthogonal axes of maximum rotational compliance. In particular, analytical results are provided to characterize the compliance behavior of the considered chain in 3D space as a function of flexure geometric parameters.

2 Formulation

A spherical flexure connecting the rigid links A and B is depicted in Fig. 1. It is a solid of revolution characterized by an annulus sector cross-section with inner and outer radii, r_i and r_o, and subtended angle β (see Fig. 2), an axis of revolution z_k

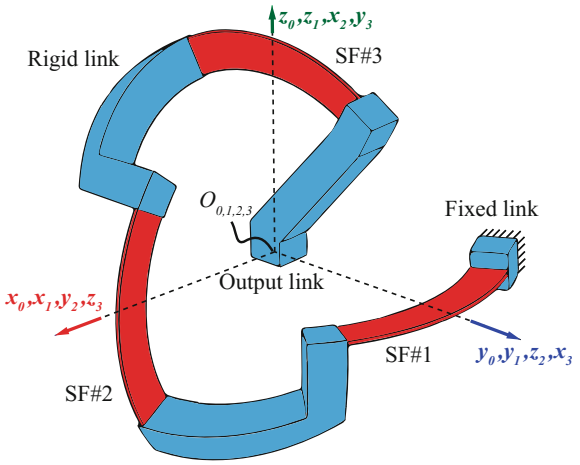

Fig. 3 SF-based compliant spherical 3R open chain

passing through the center O_k of the annulus and orthogonal to the cross-section axis of symmetry, **m**, (see Fig. 1), and revolution angle θ (which describes the flexure length). Cross-section dimensionless parameters, β and w^* ($w^* = \frac{r_o - r_i}{r_o}$), are such that its smaller area moment of inertia is in the direction of the **m** axis. Assuming link A being clamped and B free and loaded, the small deflection behavior of the flexure about its unloaded configuration can be described by the following relation [23]:

$$ {}^k\mathbf{s} = \begin{bmatrix} {}^k\mathbf{u} \\ \hdashline {}^k\boldsymbol{\theta} \end{bmatrix} = \begin{bmatrix} {}^k\mathbf{C}_{uf} & {}^k\mathbf{C}_{um} \\ \hdashline {}^k\mathbf{C}_{\theta f} & {}^k\mathbf{C}_{\theta m} \end{bmatrix} \cdot \begin{bmatrix} {}^k\mathbf{f} \\ \hdashline {}^k\mathbf{m} \end{bmatrix} = {}^k\mathbf{C} \cdot {}^k\mathbf{w} \tag{1} $$

where ${}^k\mathbf{s}$ is composed of an incremental translation ${}^k\mathbf{u} = [{}^k u_x \;\; {}^k u_y \;\; {}^k u_z]^T$ and an incremental rotation ${}^k\theta = [{}^k\theta_x \;\; {}^k\theta_y \;\; {}^k\theta_z]^T$, ${}^k\mathbf{w}$ is composed of an incremental force ${}^k\mathbf{f} = [{}^k f_x \;\; {}^k f_y \;\; {}^k f_z]^T$ and an incremental torque ${}^k\mathbf{m} = [{}^k m_x \;\; {}^k m_y \;\; {}^k m_z]^T$, whereas ${}^k\mathbf{C}_{uf}$, ${}^k\mathbf{C}_{um}$, ${}^k\mathbf{C}_{\theta f}$, ${}^k\mathbf{C}_{\theta m}$ are three-dimensional matrices composed of entries with dimensions [m/N], [1/N], [rad/N], and [rad/Nm] respectively.

As a consequence, ${}^k\mathbf{C} \equiv {}^k C_{ij}$ is a 6×6 matrix with entries of non uniform physical dimensions, the submatrices ${}^k\mathbf{C}_T = [{}^k\mathbf{C}_{uf} \;\; {}^k\mathbf{C}_{um}]$ and ${}^k\mathbf{C}_R = [{}^k\mathbf{C}_{\theta f} \;\; {}^k\mathbf{C}_{\theta m}]$ relating the external wrench to the resulting translations and rotations respectively.

The expression of Eq. 1 is frame dependent. For any SF intended for spherical motion about the center of its centroidal axis circle, a suitable frame is S_k that features center at O_k and orthogonal axes x_k, y_k and z_k respectively lying on centroidal axis plane, on beam symmetry plane and along the intersection of these two planes (see Fig. 1). In this frame, indeed, sub-matrices ${}^k\mathbf{C}_{uf}$ and ${}^k\mathbf{C}_{\theta m}$ are diagonal (meaning that x_k, y_k and z_k are along the principal directions of rotational and translational compliance of the flexure), and the components of ${}^k\mathbf{C}_{uf}$ and ${}^k\mathbf{C}_{um}$ (or ${}^k\mathbf{C}_{\theta f}$) indicate how the desired center of spherical motion drifts as a consequence of applied external forces and torques.

Knowing matrix ${}^{k}\mathbf{C}$ for a single spherical flexure, the compliance matrix of the in-series ensemble of any number n of identical flexures can be obtained with the following formula [2]:

$$ {}^{0}\mathbf{C} = \sum_{k=1}^{n} {}^{0}\mathbf{T}_{k}^{-T} \cdot {}^{k}\mathbf{C} \cdot {}^{0}\mathbf{T}_{k}^{-1} = \sum_{k=1}^{n} {}^{k}\mathbf{T}_{0}^{T} \cdot {}^{k}\mathbf{C} \cdot {}^{k}\mathbf{T}_{0} \tag{2} $$

where ${}^{k}\mathbf{T}_{0}$ is a 6×6 matrix to transform the components of the stiffness matrix ${}^{k}\mathbf{C}$ of the k–th flexure from the local frame S_k to a ground frame S_0. In particular, the expression of ${}^{k}\mathbf{T}_{0}$ is:

$$ {}^{k}\mathbf{T}_{0} = \left[\begin{array}{c:c} {}^{k}\mathbf{R}_{0} & \mathbf{0} \\ \hdashline {}^{k}\widetilde{\mathbf{r}}_{0} \cdot {}^{k}\mathbf{R}_{0} & {}^{k}\mathbf{R}_{0} \end{array}\right] = \left[\begin{array}{c:c} {}^{0}\mathbf{R}_{k}^{T} & \mathbf{0} \\ \hdashline \left({}^{0}\widetilde{\mathbf{r}}_{k} \cdot {}^{0}\mathbf{R}_{k}\right)^{T} & {}^{0}\mathbf{R}_{k}^{T} \end{array}\right] \tag{3} $$

where ${}^{k}\mathbf{R}_{0}$ denotes the rotation matrix of frame S_0 with respect to frame S_k and ${}^{0}\widetilde{\mathbf{r}}_{k}$ indicating the skew symmetric matrix of the position vector ${}^{k}\mathbf{r}_{0}$, which locates the origin of frame S_0 with respect to frame S_k.

For the compliant spherical 3R chain shown in Fig. 3, made by three identical spherical flexures with coincident centers O_k and mutually orthogonal axes, the overall compliance matrix expressed with respect to the reference frame of the first spherical flexure (namely, $S_0 \equiv S_1$) results as [24]:

$$ {}^{0}\mathbf{C}^{3\mathrm{R}} = \begin{bmatrix} C_{x,f_x} & 0 & 0 & 0 & C_{x,m_y} & C_{x,m_z} \\ 0 & C_{y,f_y} & 0 & C_{y,m_x} & 0 & C_{y,m_z} \\ 0 & 0 & C_{z,f_z} & C_{z,m_x} & C_{z,m_y} & 0 \\ 0 & C_{\theta_x,f_y} & C_{\theta_x,f_z} & C_{\theta_x,m_x} & 0 & 0 \\ C_{\theta_y,f_x} & 0 & C_{\theta_y,f_z} & 0 & C_{\theta_y,m_y} & 0 \\ C_{\theta_z,f_x} & C_{\theta_z,f_y} & 0 & 0 & 0 & C_{\theta_z,m_z} \end{bmatrix}_{3\mathrm{R}} \tag{4} $$

where:

$$ \begin{aligned} C_{x,f_x} &= C_{y,f_y} = C_{z,f_z} = \frac{R\theta\left(I_n GJ + GJR^2A + R^2EAI_n\right)}{EAI_n GJ} = C_t \\ C_{\theta_x,m_x} &= C_{\theta_y,m_y} = C_{\theta_z,m_z} = \frac{R\theta\left(I_n EI_m + I_n GJ + GJI_m\right)}{GJEI_m I_n} = C_r \\ C_{x,m_y} &= C_{y,m_z} = C_{z,m_x} = C_{\theta_x,f_z} = C_{\theta_y,f_x} = C_{\theta_z,f_y} = \frac{-2R^2\sin(\theta/2)}{GJ} = C_{tr_1} \\ C_{x,m_z} &= C_{y,m_x} = C_{z,m_y} = C_{\theta_x,f_y} = C_{\theta_y,f_z} = C_{\theta_z,f_x} = \frac{2R^2\sin(\theta/2)}{EI_n} = C_{tr_2} \end{aligned} \tag{5} $$

In Eq. 5, E and G are the Young's and shear moduli of the employed material. A, R, I_m, I_n and J are, respectively, cross section area, centroidal axis radius, area moments of inertia and torsional constant of the flexure cross section (refer to Fig. 2) that read as follows [25]:

$$A = \frac{r_o^2\beta}{2} - \frac{r_i^2\beta}{2} = \frac{(r_o^2 - r_i^2)\beta}{2} \tag{6}$$

$$R = \frac{4}{3}\frac{(r_o^3 - r_i^3)\sin\beta/2}{(r_o^2 - r_i^2)\beta} \tag{7}$$

$$I_m = \frac{1}{8}(r_o^4 - r_i^4)(\beta - \sin\beta) \tag{8}$$

$$I_n = \frac{1}{8}(r_o^4 - r_i^4)(\beta + \sin\beta) - \frac{8}{9}\frac{(r_o^3 - r_i^3)^2\sin^2(\beta/2)}{(r_o^2 - r_i^2)\beta} \tag{9}$$

$$J = \frac{2}{3}\sin^3(\beta/2)(r_o^4 - r_i^4) - 16\sin^4(\beta/2)(V_L r_o^4 + V_S r_i^4) \tag{10}$$

where:

$V_L = 0.10504 - 0.2\sin(\beta/2) + 0.3392\sin^2(\beta/2) - 0.53968\sin^3(\beta/2) + 0.82448\sin^4(\beta/2)$
$V_S = 0.10504 + 0.2\sin(\beta/2) + 0.3392\sin^2(\beta/2) + 0.53968\sin^3(\beta/2) + 0.82448\sin^4(\beta/2)$

Equation 10 is the formula for the torsional constant firstly proposed by J.B. Reynolds to account for the warping of annulus sector cross-sections [15, 16].

As one can notice from Eqs. 4 and 5, the compliance matrix of the compliant spherical 3R chain with respect to frame S_0 still retains diagonal translational and rotational sub-matrices (${}^0\mathbf{C}_{uf}$ and ${}^0\mathbf{C}_{\theta m}$), and is only a function of four independent factors: C_t, C_r, C_{tr_1} and C_{tr_2}. C_r is the primary rotational compliance of the 3R chain, which should be as high as possible to minimize resistance to desired spherical motions. C_t is a secondary translational compliance, which should be as close as possible to zero to minimize drift of the desired center of spherical motion (O_0) under the action of the force vector ${}^0\mathbf{f}$ applied on the end-link. C_{tr_1} and C_{tr_2} are secondary coupled rotational-translational compliances, which should be as close as possible to zero to minimize spherical motion center drift under the action of the torque vector ${}^0\mathbf{m}$ applied on the end-link.

3 Parametric Evaluation of the Compliant Spherical 3R Chain

This section investigates the influence of flexure geometry on the ability of the considered 3R chain in the generation of spherical motions. The study is performed by evaluating the following three indices:

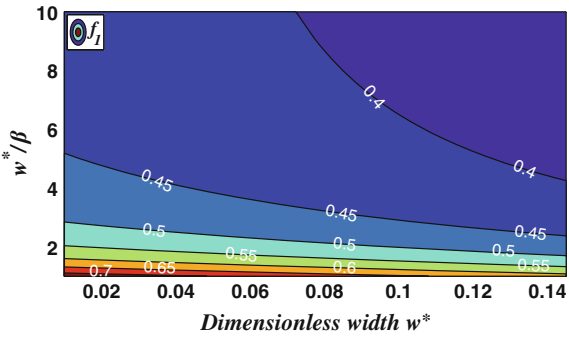

Fig. 4 The influence of varying w^* and w^*/β on f_1

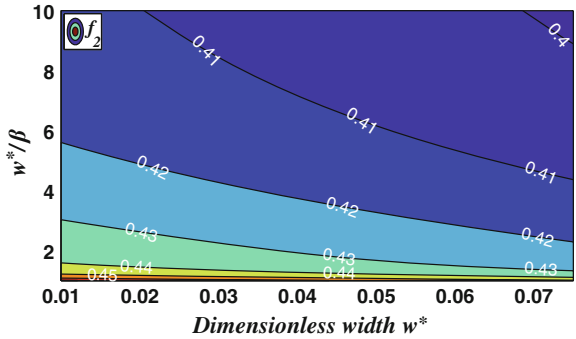

Fig. 5 The influence of varying w^* and w^*/β on f_2 for $\theta = 45°$

$$f_1 = \left| \frac{1}{r_o^2} \frac{C_t}{C_r} \right| \qquad f_2 = \left| \frac{1}{r_o} \frac{C_{tr_1}}{C_r} \right| \qquad f_3 = \left| \frac{1}{r_o} \frac{C_{tr_2}}{C_r} \right| \tag{11}$$

that represent the dimensionless ratios of the translational and coupled translational-rotational compliances of a generic compliant spherical 3R chain to the rotational counterpart. In the definition of these indices, the curvature radius r_o of the SF is used as characteristic size to obtain scale-independent expressions that only depend on the flexure shape dimensionless parameters w^*, β and θ. In particular, f_1 is only a function of w^* and w^*/β, whereas f_2 and f_3 also depend on θ. Among the possible choices, r_o has been chosen as characteristic length since it describes the overall encumbrance of the 3R chain, which is often the most important application constraint in the design optimization process. Plots of Eq. 11 are reported in Figs. 4, 5, 6, 7 and 8 as a function of the SF aspect ratios w^* and w^*/β. The dependency of f_2 and f_3 on θ is shown by comparing Figs. 5 and 7 (for $\theta = 45°$) to Figs. 6 and 8 (for $\theta = 90°$). In addition, the contour plot of the size independent factor $C_r^* = C_r * r_o^3/\theta$ (which is constant irrespective of the value of θ and only dependent on the cross section aspect ratios w^* and w^*/β) is reported in Fig. 9. As figures show, maximization of